AIAA 80-1596R

Optimization of Tactical Aircraft Maneuvers Utilizing High Angles of Attack

K.H. Well*
DFVLR, Oberpfaffenhofen, Federal Republic of Germany
B. Faber†
Messerschmitt-Bölkow-Blohm (MBB), Ottobrunn, Federal Republic of Germany
and
E. Berger‡
DFVLR, Oberpfaffenhofen, Federal Republic of Germany

Future high-performance aircraft will have high thrust/weight ratios, will be equipped with control-configured vehicle technology, will be extremely lightweight, and possibly have the capability of flying at very high angles of attack in the "poststall" region. This paper investigates, by using numerical optimization techniques, whether the poststall capability improves performance for several tactical maneuvers. Specifically, minimum-time turning maneuvers for a variety of boundary conditions and flight-path constraints are computed 1) for aircraft A which has poststall capability and 2) for aircraft B which does not, but is otherwise identical to A. It is concluded that for two combinations of boundary conditions/path constraints, flight time can be reduced if high angles of attack are utilized. In the majority of cases, however, minimum-time maneuvers are flown, load constraints permitting, at or near the maximum lift coefficient.

Nomenclature

a = velocity of sound/coefficient of polynomial
b = coefficient of polynomial
c = coefficient of polynomial/vector of constraints
C_D = drag coefficient
C_L = lift coefficient
C_T = thrust coefficient
$C_{\dot{m}}$ = specific fuel consumption coefficient
D = aerodynamic drag force
d = distance between pursuer and evader
g = acceleration of gravity
h = altitude
H = variational Hamiltonian
L = Lagrangian function/lift force
m = aircraft mass/number of control functions
M = Mach number
N = resulting force normal to flight path
n = number of state variables
nzcl = number of coefficients of numerator polynomial for $C_L(\alpha)$
nzcd = number of coefficients of numerator polynomial for $C_D(\alpha)$
nncl = number of coefficients of denominator polynomial for $C_L(\alpha)$
nncd = number of coefficients of denominator polynomial for $C_D(\alpha)$
nctm = number of coefficients of polynomial in M for C_T
ncth = number of coefficients of polynomial in h for C_T
ncmh = number of coefficients of polynomial in h for $C_{\dot{m}}$
ncmm = number of coefficients of polynomial in M for $C_{\dot{m}}$
ncmd = number of coefficients of polynomial in δ for $C_{\dot{m}}$
n_z = load factor in direction of z axis (body axes)
n_{za} = load factor normal to flight path
q = number of final conditions
S = reference area
T = resulting force tangential to flight path
T_T = thrust
T_P = thrust of pursuer
u = control vector of optimal control problem
V = aircraft true airspeed
x = state vector of optimal control problem
x_g, y_g, z_g = geodetic coordinates, ground axis system
y = vector of decision variables
α = angle of attack
β = aspect angle
γ = flight-path angle
δ = power setting
ζ, κ = auxiliary state variables
η_K = speed brake angle
ϑ = vector in NLP algorithm
σ = matrix of penalty constants
θ = pitch angle (body axes)
λ, ν = Lagrange multipliers
μ = velocity bank angle
Φ = bank angle (body axes)/cost function
φ = vector of right-hand sides
χ = velocity yaw angle
ρ = density of atmosphere
Ψ = yaw angle (body axes)
ψ = vector of boundary conditions

Subscripts

ref = reference value
0,f = initial, final value
1,2,3 = engine states
H = auxiliary variable/horizontal
max,min = maximum, minimum values
P = pursuer
E = evader
V = vertical

Presented as Paper 80-1596 at the AIAA Atmospheric Flight Mechanics Conference, Danvers, Mass., Aug. 6-8, 1980; submitted Oct. 15, 1980; revision received May 18, 1981.

*Research Scientist, Institute for Flight Systems Dynamics. Member AIAA.
†Research Engineer, Aircraft Division.
‡Program Analyst, Institute for Flight Systems Dynamics.

Introduction

IN the early phase of the development of a new tactical fighter aircraft, the analyst was asked if the performance of the planned aircraft would be improved by providing it with the capability of flying at very high angles of attack in the "poststall" (PST) mode. It was decided to answer the question in two ways: 1) by conducting air combat simulations in a manned simulator with two aircraft participating, aircraft A with PST capability and aircraft B without, where the advantages and disadvantages of the PST capability were judged by the two participating pilots, and 2) by using trajectory optimization methods with essentially identical mathematical models to those used in the manned simulations. Advantages and disadvantages of the PST capability were obtained by comparing optimal trajectories of both aircraft for several typical flight maneuvers. While the first approach is more general as far as evaluating the overall performance is concerned, the second approach is more methodical and provides precise numerical data about advantages and also clear interpretations.

This paper deals with the second approach only. It is a summary of Ref. 1 and is divided into three parts. The first part contains a description of the point-mass equations for three-dimensional flight, a presentation of typical aerodynamic data for a PST aircraft, typical engine data, and the approximation of those data using rational functions.

The second part gives a brief description of the numerical optimization method used, namely parameterization of the control functions of the optimal control problem and solution of the resulting nonlinear programming problem via multiplier methods.

In the third part, several turning maneuvers with different boundary conditions are discussed. Since minimum time turns are most important for air combat maneuvers, flight time was used as a cost function in all cases. With given initial state, first the minimum time turning maneuvers (TM's) are computed for 1) free final state, 2) free final state except altitude prescribed, 3) fixed final state, and 4) free final state with fuselage direction prescribed (fuselage pointing). Next, a slicing maneuver (SM) is computed. It consists of two sequential minimum time TM's in the opposite direction with the additional constraint that the fuselage attitude should be positive at all times. This constraint guarantees certain visibility conditions for the pilot. Last, two optimal evasive maneuvers (EM's) are presented with two participating aircraft. Here, the objective was to find out if aircraft A can evade a pursuer flying strictly according to a pure pursuit guidance law. The first EM with the relative heading of both aircraft of 90 deg, the second EM with 0 deg. All numerical results will be discussed and summarized in the conclusion.

Equations of Motion

System Equations

The three-dimensional motion of a point-mass vehicle over a flat, nonrotating Earth assuming no sideslip is described by the differential quations[2]:

$$\begin{aligned} m\dot{V} &= T - mg\sin\gamma \\ mV\dot{\chi} &= N\sin\mu/\cos\gamma \\ mV\dot{\gamma} &= N\cos\mu - mg\cos\gamma \\ \dot{x}_g &= V\cos\gamma\cos\chi \\ \dot{y}_g &= V\cos\gamma\sin\chi \\ -\dot{h} = \dot{z}_g &= -V\sin\gamma \\ \dot{m} &= -C_{\dot{m}}T_T \end{aligned} \tag{1}$$

with

$$T = T_T\cos\alpha - D \qquad N = T_T\sin\alpha + L \tag{2}$$

The aerodynamic and propulsive forces are determined by the following equations:

$$\begin{aligned} T_T &= C_T(h,M,\delta)\,T_{\text{ref}} \\ L &= C_L(\alpha,M)\rho(h)SV^2/2 \\ D &= C_D(\alpha,\eta_K,M)\rho(h)SV^2/2 \end{aligned} \tag{3}$$

with the Mach number $M = V/a(h)$. For given control function $\alpha(t),\mu(t),\delta(t),\eta_K(t)$ and for given initial state variables $V_0,\chi_0,\gamma_0,x_{g0},y_{g0},z_{g0},m_0$, the system, Eq. (1), can be integrated and has a unique solution.

For the two evasive maneuvers, it is assumed that a pursuer (subscript P) with the same aerodynamic and propulsive characteristics follows aircraft A. The pursuer is steering his aircraft according to a pure pursuit guidance law, that is, the velocity vector of P always points toward A. This guidance law, together with the assumption $T_P = T_{T\max}$, determines the control actions of P completely (for details see Ref. 1). The motion of P can be described by solving seven additional differential equations for the additional state variables: the distance d between P and A; the velocity of the pursuer, V_P; azimuth χ_P and path inclination γ_P of pursuer; and the geodetic coordinates of the pursuer, x_P, y_P, and h_P. With given time histories of the control functions of A and seven initial values, the additional differential equations can be integrated.

Approximation of Data

The aerodynamic and propulsive coefficients $C_L,C_D,C_T,C_{\dot{m}}$ are functions of several variables and are given in tabular form. In order to apply any of the existing optimization algorithms, these data must be approximated by sufficiently differentiable functions. For the sample aircraft, the aerodynamic coefficients are given as

$$C_L(\alpha), C_D = C_{D0}(\alpha) + C_{DK}(\eta_K,M) \tag{4}$$

where C_{D0} is the drag coefficient for $\eta_K = 0$ and C_{DK} the additional one due to speed brakes $\eta_K \neq 0$. The thrust coefficient is given for three engine states, namely, $C_{Tl}(h,M)$ for "idle," $C_{T2}(h,M)$ for maximum "normal power," and $C_{T3}(h,M)$ for maximum "afterburner." "Idle" is defined as $0.1 * C_{T2}(h,M)$. In between the engine states, C_T depends linearly on δ. Specific fuel consumption is given for "normal power," $C_{\dot{m}2}(h,M,\delta)$, and for "afterburner," $C_{\dot{m}3}(h,M,\delta)$. To have an analytical expression for the dependence on power setting, we define

$$C_T = a\delta^2 + b\delta + c \tag{5}$$

where the coefficients a,b,c are determined from

$$\begin{aligned} C_T(h,M,0.1) &= C_{Tl}(h,M) \equiv 0.1C_{T2}(h,M) \\ C_T(h,M,1) &= C_{T2}(h,M) \\ C_T(h,M,2) &= C_{T3}(h,M) \end{aligned} \tag{6}$$

resulting in

$$a = (C_{T3} - 2C_{T2})/1.9 \qquad b = C_{T2} - 1.1a \qquad c = 0.1a \tag{7}$$

The aerodynamic coefficients are approximated using the rational functions:

$$C_L = \sum_{i=1}^{nzcl} a_i \alpha^{nzcl-i} \Big/ \sum_{j=1}^{nncl} b_j \alpha^{nncl-j}$$
$$C_{D0} = \sum_{i=1}^{nzcd} a_i \alpha^{nzcd-i} \Big/ \sum_{j=1}^{nncd} b_j \alpha^{nncd-j} \tag{8}$$

and a polynomial for C_{DK}:

$$C_{DK} = (a_1 \eta_K^2 + a_2 \eta_K)(M + a_3) \tag{9}$$

The engine data are approximated with polynomials:

$$C_{Ti} = \sum_{j=1}^{ncth} \sum_{k=1}^{nctm} a_{jk} M^{nctm-k} h^{ncth-j} \qquad (i=2,3)$$
$$C_m = \sum_{i=1}^{ncmd} \sum_{j=1}^{ncmh} \sum_{k=1}^{ncmm} a_{ijk} M^{ncmm-k} h^{ncmh-j} \delta^{ncmd-i} \tag{10}$$

The polynomial coefficients are determined by fitting the tabular data to the functions above, which leads to the solution of a nonlinear least-square problem for determining the coefficients in Eqs. (8) and to the solution of a linear least-square problem for the coefficients in Eqs. (9) and (10).

Typical degrees of the approximating polynomials are given in Table 1. Figure 1 shows the graphs of Eqs. (8) and the given data points. Figure 2 shows thrust coefficients and specific fuel consumption vs altitude and Mach number for two engine states with linear interpolation between the data points. Accuracy of the approximation with Eqs. (10) is near 5% for a specially selected range of independent variables.

Control Constraints

The control variables α, δ, and η_K are constrained by their minimum and maximum values. By introducing new control variables (subscript H) and with the relations

$$\alpha = \alpha_{\min} + (\alpha_{\max} - \alpha_{\min}) \sin^2 \alpha_H$$
$$\delta = \delta_{\min} + (\delta_{\max} - \delta_{\min}) \sin^2 \delta_H \tag{11}$$
$$\eta_K = \eta_{K\min} + (\eta_{K\max} - \eta_{K\min}) \sin^2 \eta_{KH}$$

the constraints are satisfied for all values of the auxiliary controls.

Constraint on Load Factor

The load factor is defined as

$$n = n_{za} = (T_T \sin\alpha + L)/mg \qquad \text{for conventional } \alpha$$
$$= n_z = (L\cos + D\sin\alpha)/mg \qquad \text{for poststall} \tag{12}$$

and constrained by its maximum value. n_z measures the acceleration in the z direction (body-fixed reference axis), which the pilot must endure during poststall maneuvers. n_{za} is the aerodynamic load factor. Both load factors have similar values for conventional flight. Numerically, a violation of the load factor constraint is avoided by defining the additional differential equation and boundary conditions

$$\dot{\zeta} = |n| - n_{\max} \qquad \text{if } |n| > n_{\max} \qquad \zeta(t_0) = 0$$
$$= 0 \qquad \text{otherwise} \qquad \zeta(t_f) = \epsilon_l \tag{13}$$

Table 1 Number of polynomial coefficients

nzcl	nncl	nzcd	nncd	ncth	nctm	ncmd	ncmh	ncmm
5	4	5	6	5	3	2	3	4

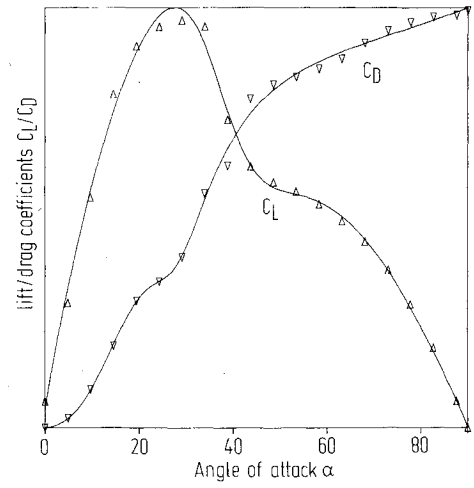

Fig. 1 Aerodynamic coefficients.

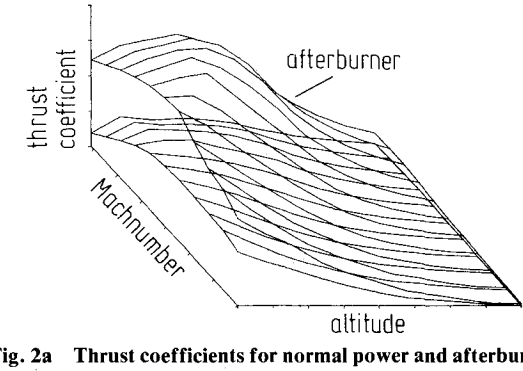

Fig. 2a Thrust coefficients for normal power and afterburner.

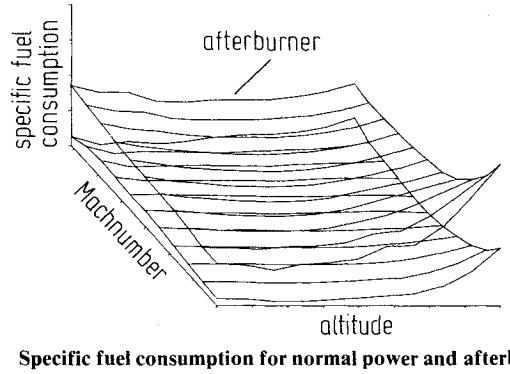

Fig. 2b Specific fuel consumption for normal power and afterburner.

Constraint on Pitch

For certain maneuvers, it is required that

$$\theta(t) \geq 0 \tag{14}$$

with

$$\sin\theta = \cos\alpha\sin\gamma + \sin\alpha\cos\mu\cos\gamma \tag{15}$$

This constraint is handled the same way as the load factor constraint by adding the new differential equation and

boundary equations

$$\begin{aligned} \dot{\kappa} &= \sin\theta \quad \text{if } \sin\theta < 0 \quad \kappa(t_0) = 0 \\ &= 0 \quad \text{otherwise} \quad \kappa(t_f) = \epsilon_2 \end{aligned} \tag{16}$$

where ϵ_1 and ϵ_2 are small preselected numbers.

Euler Angles

Besides velocity yaw angle χ, velocity pitch angle γ, and velocity bank angle μ, it is useful to have the yaw angle Ψ, the bank angle Φ, and the pitch angle θ. These angles are obtained by comparing coefficients of angular rotations from body axes to ground axes (subscript g) with those from body axes to wind axes to ground axes (see Ref. 2). The result is

$$\tan\theta = \frac{\sin\mu\cos\gamma}{-\sin\alpha\sin\gamma + \cos\alpha\cos\mu\cos\gamma} \tag{17a}$$

$$\tan\Psi = \frac{\cos\alpha\cos\gamma\sin\chi - \sin\alpha(\cos\mu\sin\gamma\sin\chi - \sin\mu\cos\chi)}{\cos\alpha\cos\gamma\cos\chi - \sin\alpha(\cos\mu\sin\gamma\cos\chi - \sin\mu\sin\chi)} \tag{17b}$$

The expression for θ is given in Eq. (15). Equations (17) are used to compute the aircraft attitude at any point along the trajectory for given control variables.

Optimal Control Problem and Numerical Method

Optimal Control Problem

The optimal control problem (OCP) of the previous section consists of finding the control functions $\alpha_H(t)$, $\mu(t)$, $\delta_H(t)$, $\eta_{KH}(t)$ for the differential systems, Eqs. (1) supplemented by Eqs. (13) and (16), and the seven additional equations for the pursuer, subject to boundary conditions that will be specified in the next section. The system is to be controlled such that the final state is reached in minimum time. With x: state vector, u: control vector, φ: vector of right-hand sides, the OCP at hand is stated as:

$$\text{minimize } \Phi(x,\pi)_1 \tag{18}$$

subject to

$$\begin{aligned} \dot{x} &= \varphi(x,u,\pi) \qquad 0 \le t \le 1 \\ x(0) &= \text{given} \qquad \psi(x,\pi)_1 = 0 \end{aligned} \tag{19}$$

It is assumed that the independent variable time t has been normalized, the parameter π (a scalar) represents the free final time t_f. Necessary conditions for optimality are

$$\begin{aligned} \dot{\lambda} &= H_x \qquad H_u = 0 \qquad 0 \le t \le 1 \\ (H_\pi) + \Phi_\pi + \psi_\pi \nu &= 0 \quad , \quad \lambda + \Phi_x + \psi_x \nu = 0 \end{aligned} \tag{20}$$

where $\lambda(t)$ and ν are Lagrange multipliers and the Hamiltonian $H = -\lambda^T \varphi$.

Numerical Solution of OCP

The most common numerical technique for solving an OCP is to parameterize the control function and solve the resulting nonlinear programming problem (NLP) using one of the many NLP solvers available (see Refs. 3-5). The method used in this paper is described in detail in Ref. 6. It consists of selecting a grid t_i, $i=1, \ldots, n_g$, using the values of the control fucntions at the grid points $u(t_i)$ as parameters of the problem, and interpolating in between using cubic spline functions. The resulting NLP consists of finding the components of the decision vector

$$y = (u_1(t_1), u_1(t_2), \ldots, u_m(t_{ng}), \pi)^T \tag{21}$$

such that

$$c_j(y) = \psi_j(x,\pi)_1 \qquad (j = 1,\ldots,q) \tag{22}$$

In addition,

$$f(y) = \Phi(x,\pi)_1 \tag{23}$$

is minimized subject to the appropriate differential system and initial conditions. Equation (23) is converted into an unconstrained problem by minimizing the Lagrangian

$$L(y,\vartheta,\sigma) = f(y) + \tfrac{1}{2}(c-\vartheta)^T \sigma (c-\vartheta) \tag{24}$$

where σ is a diagonal $q \times q$ matrix of penalty constants and ϑ, a q vector of an outer iteration loop. The NLP algorithm consists of the following steps:

1) Select y^0, ϑ^1, σ^1.

2) Set $k = k+1$ and $y^k = \arg\min L(y, \vartheta^k, \sigma^k)$.

3) If $\|c^k\| < \|c^{k-1}\| \cdot \rho$, where $0 < \rho < 1$, then $\vartheta^{k+1} = \vartheta^k - c(y^k)$ and $\sigma^{k+1} = \sigma^k$. Otherwise, $\vartheta^{k+1} = \vartheta^k$ and $\sigma^{k+1} = \eta\sigma^k$, where $\eta > 1$.

4) If $\|c^k\| < \epsilon_1$ and $\|L_y^k\| \le \epsilon_2$ stop. Otherwise, go to step 2.

The differential system is always satisfied by using a Runge-Kutta 7/8th-order initial value solver. In minimizing L, partial derivatives with respect to y are needed. In this paper they are computed using impulsive response functions as suggested in Refs. 4 and 6.

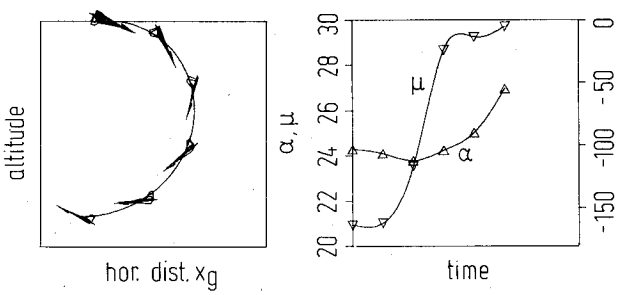

Fig. 3 Free turning maneuver ($V_0 = 100$ m/s).

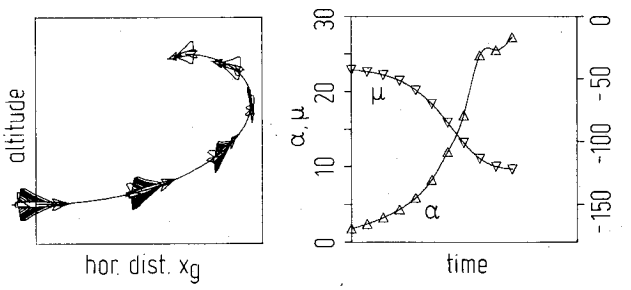

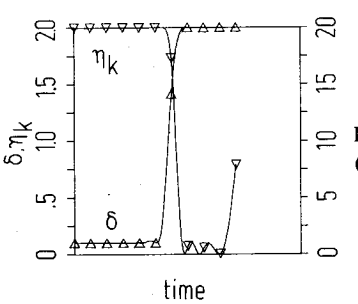

Fig. 4 Free turning maneuver ($V_0 = 300$ m/s).

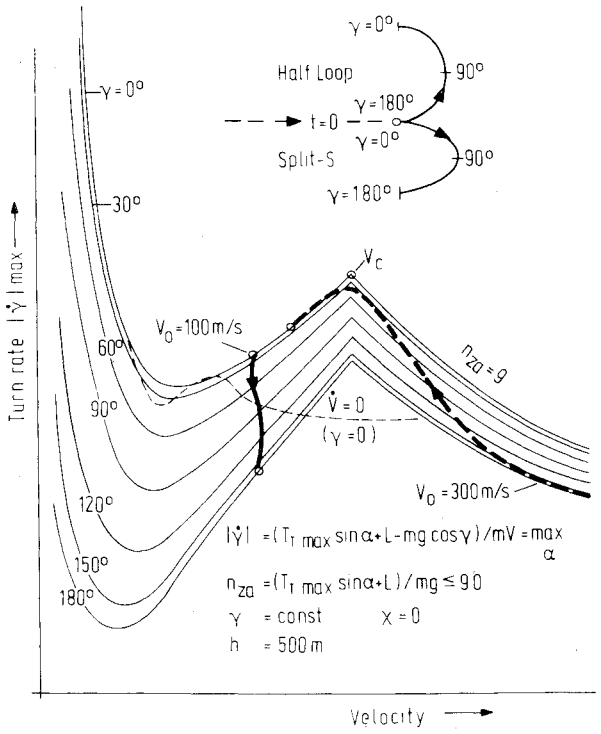

Fig. 5 Free turning maneuver in $|\dot{\gamma}|_{max}$ (V,γ) diagram.

Minimum-Time Maneuvers

Turning Maneuvers

All turning maneuvers are characterized by the boundary conditions V_0 and $\chi_0 = 0$ deg, $\gamma_0 = 0$ or 180 deg, x_{g0}, y_{g0}, $x_f = 180$ or 0 deg, and $\gamma_f = 0$ or 180 deg. The convention adopted is given in the inset in Fig. 5. In the vertical plane, maneuvers are started with $\chi_0 = 0$ deg, $\gamma_0 = 180$ deg if a half-loop is executed; they are started with $\chi_0 = 0$ deg, $\gamma_0 = 0$ deg if a split-S is executed. Three-dimensional maneuvers are always with $\chi_0 = 0$ or 180 deg and $\gamma = 0$ deg.

Free turning has no additional boundary conditions. Final velocity and altitude are selected optimally. Figures 3 and 4 show trajectories and control actions for $V_0 = 100$ and 300 m/s. Figure 5 depicts the maneuvers in a $|\dot{\gamma}|_{max} - V$ diagram.

The diagram is valid for flight in the vertical plane (half-loop or split-S) and shows maximum instantaneous "turn rates" $|\dot{\gamma}|$ as a function of velocity and path inclination subject to a load factor constraint. The highest "turn rate" outside the poststall region is achieved at $V = V_c$, V_c being the corner velocity. Inside the poststall region extremely high turn rates can be achieved. During a half-loop (from $\gamma = 180 \rightarrow 0$ deg)—executed at constant speed—"turn rates" increase. During a split-S ($\gamma = 0 \rightarrow 180$ deg), turn rates decrease due to the gravitational acceleration. Also depicted is the maximum turn rate for $\dot{V} = 0$. The diagram shows the sequence of states for the optimal maneuvers. For $V_0 = 100$ m/s, the optimal maneuver is a split-S flown at nearly constant velocity. In contrast to an exactly constant speed maneuver, which would not be as fast, the angle of attack is less than 27 deg in the beginning in order not to decelerate too much, resulting in a decreased turn rate. Only at the end of the maneuver is $\alpha = 27$ deg achieved (see also Fig. 4). For $V_0 = 300$ m/s, the maneuver starts at the aerodynamic load limit. In order to fly at high turn rates, the velocity is initially decreased ($\delta = 0.1$, $\eta_K = \eta_{K\max}$). Before reaching the corner velocity however, $\delta = 2$ and $\eta_K = 0$ is the optimal control action. The maneuver tends toward a half-loop. Here, the gravitational force assists the deceleration process necessary in order to fly near the corner velocity. Since the trajectory is not exactly in the vertical plane, the maneuver has a dotted line.

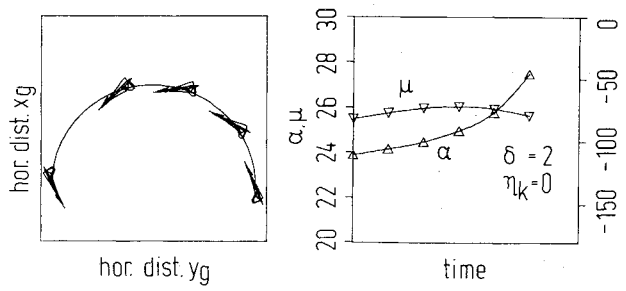

Fig. 6 Turning maneuver, final altitude prescribed ($V_0 = 100$ m/s).

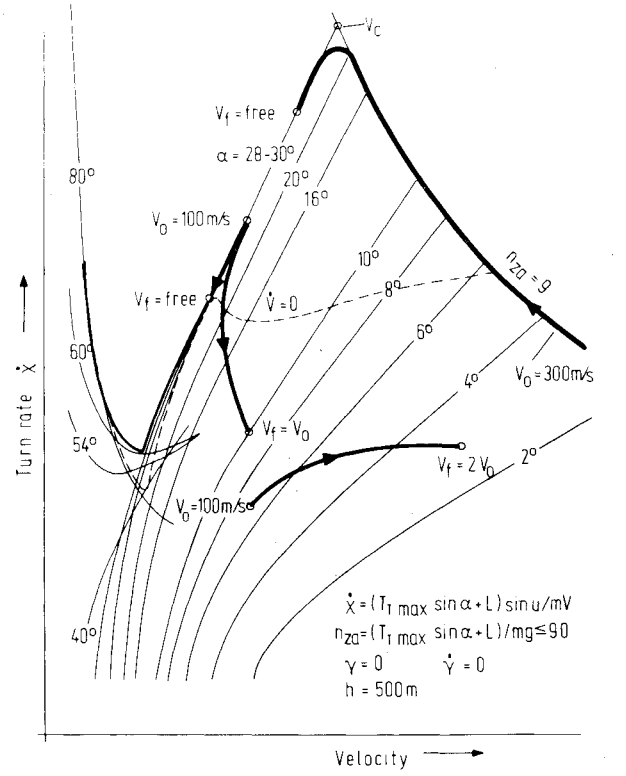

Fig. 7 Turning maneuver in $\dot{\chi}(V)$ diagram.

A turning maneuver with prescribed final altitude is shown in Fig. 6. The maneuver is flown mainly in the horizontal plane with α near $C_{L\max}$. Figure 7 shows various maneuvers in the $\dot{\chi} - V$ diagram.

The digram illustrates instantaneous turn rates in the horizontal plane subject to the load factor constraint. The highest turn rates are again achieved at $V = V_c$ and in the poststall region. Also shown is the turn rate for $\dot{V} = 0$. For $V_0 = 100$ m/s, the optimal maneuver is flown along the $\dot{\chi}_{max}$ boundary, final velocity being somewhat smaller than V_0. For $V_0 = 300$ m/s, the maneuver begins at the load limit boundary. Throttle setting and speed brakes are used in the same way as for the maneuver in the vertical plane. The maneuver ends at a smaller velocity than V_c on the $\dot{\chi}_{max}$ boundary. Depicted, in addition, are two maneuvers with final altitude and velocity prescribed. Here, the high angle-of-attack time history of the corresponding maneuver with free final velocity and fixed final altitude is modified such that at the end α is decreased to about 10 deg. For $V_f = 2 * V_0$ the angle-of-attack time history varies from about 7 to 3 deg.

Control time histories and trajectories of aircrafts A and B with $\alpha_{max} = 90$ deg and 30 deg, respectively, where final velocity, altitude, and path coordinates are prescribed are shown in Fig. 8.

A has a time advantage over B of 12%. The optimal maneuver for A consists of a pullup maneuver, a roll from

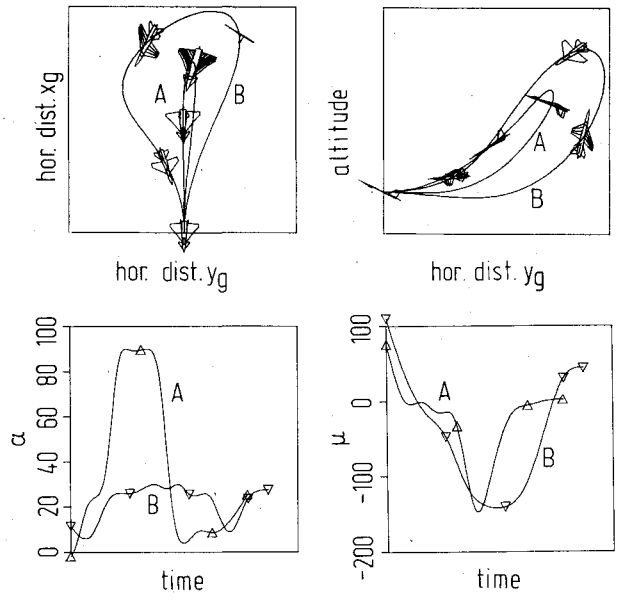

Fig. 8 Turning maneuver with final altitude, velocity, path coordinates prescribed (striped wing area indicates aircraft viewed from bottom).

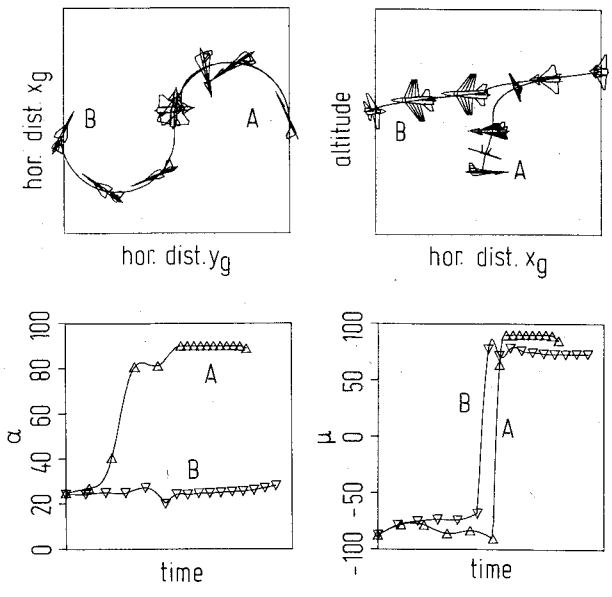

Fig. 10 Slicing maneuver (striped wing area indicates aircraft viewed from bottom).

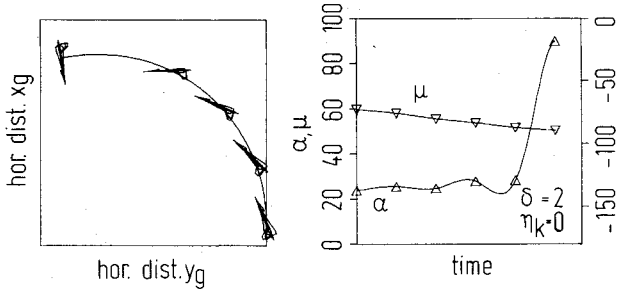

Fig. 9 Pointing maneuver ($V_0 = 100$ m/s).

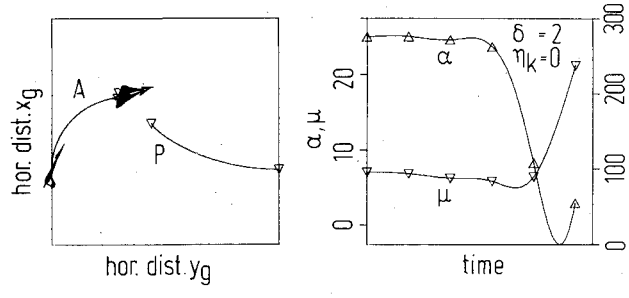

Fig. 11 Evasive maneuver with pursuer coming from the side ($\chi_0 - \chi_{P0} = 90$ deg).

head down to head up position, and a return to the initial position. The optimal maneuver for B consists of a turn to the right, to the left, and at the end, to the right again. The maneuver for A is executed mainly in the vertical plate, while B flies a three-dimensional path. Besides time advantages, A also needs less "space" for the maneuver.

Pointing Maneuver

This maneuver shows the pointing capability of A. It is assumed that two aircraft pass each other at time t_0 in opposite direction at x_{g0}, y_{g0}, h_0 (see Fig. 9). Aircraft E (evader) continues flying in $(-x_g)$ direction with constant speed V_E ($\dot{x}_E(t) = -V_E$, $y_E(t) = \text{const}$, $h_E(t) = \text{const}$). Aircraft A, the pursuer, is to point the fuselage toward E in minimum time. The corresponding boundary conditions are:

$$\begin{aligned} \cos\Psi_f + (x_{gf} - x_E(t_f))/r_H &= 0 \\ \sin\Psi_f + (y_{gf} - y_{g0})/r_H &= 0 \\ \cos\theta_f - r_H/r_V &= 0 \\ \sin\theta_f + (h_f - h_0)/r_V &= 0 \end{aligned} \tag{25}$$

with $r_V = \sqrt{r_H^2 + (h_f - h_0)^2}$ and θ, Ψ from Eqs. (15) and (17b). Figure 9 shows the control time histories and the trajectory in the horizontal plane. For $V_0 = 100$ m/s, the maneuver consists of a turn with α near $C_{L\max}$ followed by a sudden pointing action of the aircraft toward E. For $V_0 > 100$ m/s, the maneuver sequences are similar.

Slicing Maneuver

The slicing maneuver consists of two turning maneuvers in opposite direction. The first part is characterized by the initial conditions $V_0 = 100$ m/s, $\chi_0 = \gamma_0 = 0$, x_{g0}, y_{g0}, and h_0. Final conditions for the first part are $\chi_{1f} = 180$ deg, $\alpha(t_{1f}) = \alpha_{\max}$, and these, of course, are also the initial conditions for the second part. The final condition for the second part is $\chi_{2f} = 0$ deg. During the second part of the maneuver $\theta \geq 0$ is required. Figure 10 shows control time histories for aircrafts A and B and the trajectories. While B flies two turns at α near $C_{L\max}$, aircraft A makes a typical PST maneuver in the second part consisting of a steep descent at very high yaw rates with $\theta \approx 0$.

The time advantage of A compared with B is 15%. If, instead of χ_{1f} and χ_{2f}, fuselage direction would have been chosen as the final conditions, time advantages would have been even greater (approximately 50%). The high yaw required for the optimal PST turn (second part), however, cannot be achieved in practice and therefore the maneuver will be slower altogether.

Evasive Maneuvers

At the beginning of the maneuvers, both aircraft A and the pursuer (subscript P) are flying at the same altitude. P has visual contact and flies either perpendicular or parallel to A. Initial conditions are defined by χ_0, χ_{P0}, γ_0, γ_{P0}, V_0, V_{P0}, h_0, h_{P0}, and d_0. The final condition $n_{Pf} = n_{\max}$ guarantees that the pursuer overshoots his target. For $V_0 = V_{P0} = 130$ m/s and

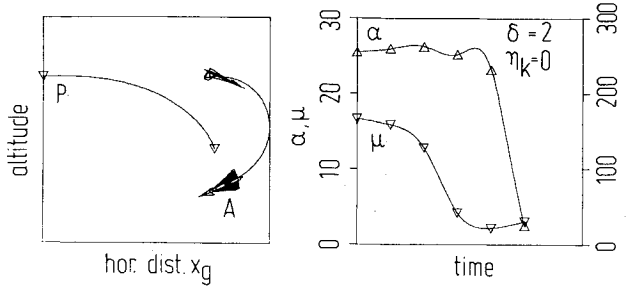

Fig. 12 Evasive maneuver with pursuer coming from behind ($\chi_0 - \chi_{P0} = 0$ deg).

$\chi_{10} - \chi_{P0} = 90$ deg, Fig. 11 shows optimal control time history and the trajectory in the horizontal plane.

The optimal evasive maneuver consists of a turn essentially in the horizontal plane with α near $C_{L\max}$. It ends with a sudden change in bank angle in opposite direction and with small angle of attack resulting in an acceleration in order to achieve a high-velocity component perpendicular to the line of sight, the final aspect ratio being approximately 90 deg. Again, the high roll rates cannot be achieved in practice, but the character of the maneuver will remain the same even if limitations are enforced.

For the same initial velocities, but $\chi_0 - \chi_{P0} = 0$, i.e., the pursuer coming from behind, the optimal evasive maneuver is shown in Fig. 12. It consists essentially of a split-S followed by an acceleration phase with small angle of attack. At the end of the maneuver, A again tries to fly perpendicular to the line of sight by changing the bank angle by 180 deg, final aspect ratio being near 90 deg too.

Conclusion

Several aircraft maneuvers have been investigated in order to determine if the poststall capability of a future tactical fighter improves performance. All maneuvers have in common that either flight-path heading or fuselage heading are to be changed in minimum time. Load factor constraints and constraints on aircraft attitude, as well as requirements on final velocity, altitude, path coordinates, load factor of the pursuing aircraft, and angle of attack characterize the maneuvers in detail. The simplifying principle that governs all optimal control actions is the tendency to fly at maximum instantaneous turn rates as long as requirements on final velocity do not correspond to smaller angles of attack. For sufficiently large initial velocities, power setting and speed brakes are used such that flight occurs near the corner velocity as much as possible because instantaneous turn rates are the highest there. Deceleration into the poststall region, where instantaneous turn rates become very large, and subsequent acceleration to the required final velocity has only been observed for one turning maneuver (fixed final state) for sufficiently small initial velocities. For the slicing maneuver, which is a typical poststall maneuver, poststall has time advantages because of the extremely large turn rates at small velocity.

In addition to time advantages due to poststall there are other advantages such as the pointing capability and the capability of maneuvering in a small area. An evaluation of these advantages is presently under way and will be reported in a future paper.

References

[1] Well, K.H., Faber, B., and Berger, E., "Optimale taktische Flugmanöver für ein Kampfflugzeug der 90er Jahre," DFVLR, FRG, Interner Bericht A552-79/6, Nov. 1979.

[2] Miele, A., *Flight Mechanics I, Theory of Flight Paths,* Addison-Wesley, Reading, Mass., 1962, pp. 42-50.

[3] Hull, D.G., "Application of Parameter Optimization Methods to Trajectory Optimization," AIAA Paper 74-825, Aug. 1974.

[4] Brusch, R.G. and Schapelle, R.H., "Solution of Highly Constrained Optimal Control Problems Using Nonlinear Programming," AIAA Paper 70-964, Aug. 1970.

[5] Gill, P.E. and Murray, W., *Numerical Methods for Optimization,* Academic Press, N.Y., 1974, pp. 219-227.

[6] Kraft, D., "FORTRAN-Programme zur numerischen Lösung optimaler Steuerungs- probleme," DFVLR, Mitteilung 80-03, March 1980.